

# Exciton Binding Energy and the Nature of Emissive States in Organometal Halide Perovskites

Kaibo Zheng, Qiushi Zhu, Mohamed Abdellah, Maria E Messing, Wei Zhang, Alexander Generalov, Yuran Niu, Lynn Ribaud, Sophie E Canton,\* Tonu Pullerits\*

## Table of Content:

1. Experimental section:.....	2
1.1 Synthesis methods:.....	2
1.2 Sample Characterizations: .....	2
1.3 Steady-state spectroscopy: .....	2
1.4 Time-resolved photoluminescence: .....	3
1.5 X-ray absorption and photoelectron spectroscopy:.....	3
2. X-ray diffraction (XRD) of MAPbBr <sub>3</sub> NPs and BCs: .....	3
3. Size and morphology of MAPbBr <sub>3</sub> nanoparticles: .....	4
4. Errors of optical band gap calculation: .....	5
5. Emission Quantum yield ( $\phi_f$ ) measurement of MAPbBr <sub>3</sub> NPs: .....	6
6. Photoionization cross-sections:.....	7
7. VB surface component:.....	7
8. XPS core level of NPs: .....	8
9. Measure the $E_b$ of BCs sample using temperature dependent photoluminescence:.....	9
10. Work function measurement:.....	9
11. Stability and reproducibility of PL kinetics: .....	10
12. Calculation of absorption coefficient and excitation density of MAPbBr <sub>3</sub> :.....	11

## Supporting information:

### 1. Experimental section:

#### 1.1 Synthesis methods

**Synthesis of precursors:** methylammonium bromide ( $\text{CH}_3\text{NH}_3\text{Br}$ ) and octylammonium bromide ( $\text{CH}_3(\text{CH}_2)_7\text{NH}_3\text{Br}$ ) were synthesized by reaction of the corresponding amine in water/HBr accordingly to the previous reports. In brief, for ( $\text{CH}_3\text{NH}_3\text{Br}$ ) 36.9 ml of HBr and 83.4 ml of  $\text{CH}_3\text{NH}_2$  were stirred for two hours in an ice bath. The resulting solution was evaporated until the formation of white crystals. These white crystals were recrystallized from ethanol solution and then used as a precursor for  $\text{CH}_3\text{NH}_3\text{PbBr}_3$  colloidal nanoparticles. The same procedures were repeated in order to prepare ( $\text{CH}_3(\text{CH}_2)_7\text{NH}_3\text{Br}$ ) where 33.5 ml of  $\text{CH}_3(\text{CH}_2)_7\text{NH}_2$  and 22.6 ml of HBr were stirred for two hours in an ice bath.

**Synthesis of  $\text{CH}_3\text{NH}_3\text{PbBr}_3$  bulk-like crystals:**  $\text{MAPbBr}_3$  microcrystals were prepared by spin coating  $\text{MAPbBr}_3$  precursors in DMF onto glass substrates with 2000 rpm of 30 sec. The substrates were then annealed in air at 85 °C for half hour to form orange colored crystals. In order to verify the crystal size, different dilution of precursors (original,  $\times 2$ ,  $\times 4$ ,  $\times 8$ ,  $\times 16$ ,  $\times 25$ ) were used which produced crystals with mean size of 14.7, 6.2, 4.2, 2.0 and 0.4  $\mu\text{m}$ , respectively.

**Synthesis of  $\text{CH}_3\text{NH}_3\text{PbBr}_3$  colloidal nanoparticles:**  $\text{CH}_3\text{NH}_3\text{PbBr}_3$  colloidal nanoparticles were synthesized via hot injection of  $\text{MABr}$ / $\text{OTABr}$  and  $\text{PbBr}_2$  precursors in non-coordinating solvent analogous to previous reports. In brief, 0.5 mmol oleic acid in 10 ml of octadecene was stirred and heated at 80 °C followed by addition of 0.3 mmol  $\text{OTABr}$  in 1 ml DMF. Then 0.2 mmol of  $\text{MABr}$  in 1 ml DMF and 0.5 mmol  $\text{PbBr}_2$  in 1 ml DMF were injected subsequently. The yellow dispersion containing nanoparticles was directly precipitated by acetone. Finally, the nanoparticles were redispersed in toluene for use. Here the ratio between  $\text{OTABr}$  and  $\text{MABr}$  is 6:4.

#### 1.2 Sample Characterizations

The morphologies of various samples were characterized via scanning electron microscopy (SEM) (Hitachi, SU8010) and high resolution analytical transmission electron microscopy (HR-TEM) (JEOL 3000F equipped with Oxford SDD x-ray analyzer).

High resolution XRD measurements were conducted at beamline 11-BM at Advanced Photon Source (APS) at Argonne National Laboratory, with the X-ray wavelength 0.414 nm (51.7 keV). Data were collected over the  $2\theta$  range from 2° to 50° in 0.001° step at ambient temperature. The GSAS software was used for indexing and determining the lattice properties. For XRD measurement, the  $\text{CH}_3\text{NH}_3\text{PbBr}_3$  powder was obtained by drying the solution of the equimolar mixture of  $\text{CH}_3\text{NH}_3\text{Br}$  and  $\text{PbBr}_2$  at 80°. The nanoparticle sample was prepared by evaporating the solvent in vacuum.

#### 1.3 Steady-state spectroscopy

Ground-state absorption spectra were measured in a UV–vis absorption spectrophotometer (PerkinElmer, Lambda 1050) equipped with integrated sphere to exclude signal due to light scattering. Steady-state photoluminescence was measured using a standard spectrometer (Horiba, Spex 1681) with excitation at 410 nm.

## 1.4 Time-resolved photoluminescence

A streak camera and time-correlated single photon counting (TCSPC) experiments were carried out. In the streak camera: the laser source is a titanium:sapphire passively mode-locked femtosecond laser (Spectra-Physics, Tsunami), emitting at 820 nm with 80 MHz repetition rate and 150 fs pulse length. The pulse repetition rate was reduced to 8 MHz via a pulse picker leaving the pulse energy unchanged. The laser pulses were frequency-doubled to 410 nm by a second-harmonic generator (Photop technologies, Tripler TP-2000B). The excitation photon flux was  $1.1 \times 10^{12}$  photons/cm<sup>2</sup>/pulse. The time-resolved photoluminescence spectra were detected in a picosecond streak camera (C6860, Hamamatsu, time resolution 1 ps) coupled to a Chromex spectrograph, triggered by the Ti:sapphire laser. A long-pass wavelength filter from 490 nm was used in front of the spectrograph to cut off the scattering from the excitation pulses.

In the time-correlated single-photon counting device (PicoQuant) a pulsed diode laser with 100k - 2.5 MHz repetition rate, was used to excite the sample at 438 nm. The interval time between pulses varied from 400 ns to 10  $\mu$ s. Long-pass wavelength filters from 520 nm were used to pick up only the band-edge emission. The emitted photons were focused onto a fast avalanche photodiode (Micro Photon Device, SPAD). The response time of the photodiode was <50 ps. The excitation photon flux was varied from  $1.0 \times 10^9 \sim 8.0 \times 10^{11}$  photons/cm<sup>2</sup>/pulse using neutral density filters.

## 1.5 X-ray absorption and photoelectron spectroscopy

X-ray photoelectron spectroscopy (XPS) and near edge X-ray absorption fine structure (NEXAFS) spectroscopy measurements were performed at beamline D1011 at MAX IV Laboratory. The photon energy used for XPS was 1000 eV, with normal emission geometry, the escape depth of the electron emitted from the valence band (VB) is  $\sim 2.5$  nm. The energy scale in the spectra was calibrated relative to Fermi level of the gold foil which was put in electrical contact with the sample. Multiple positions on the sample were measured to prove the homogeneity of the film. At each position, more than twenty scans were recorded and compared. No charging or beam-induced sample decomposition effects were detected in the spectra. NEXAFS spectra were recorded in the total electron yield mode. For both XPS and NEXAFS, the samples were deposited onto fluorine doped tin oxide (FTO) glass substrates.

## 2. X-ray diffraction (XRD) of MAPbBr<sub>3</sub> NPs and BCs

The X-ray diffraction (XRD) pattern of both samples (Fig. S1) correspond to perovskite-type structure crystallized in the cubic space group Pm-3m at ambient conditions. The XRD pattern of the NPs has clear peaks that match with the BCs. There is only a minor extra component at  $2\theta \sim 3.7^\circ$  suggesting a small contribution of impurities in the sample. The absence of significant broadening in the XRD peaks of the NPs indicates good crystalline order. The lattice constants for the BCs and the NPs are 5.9296(1) Å and 5.9266(1) Å, respectively.

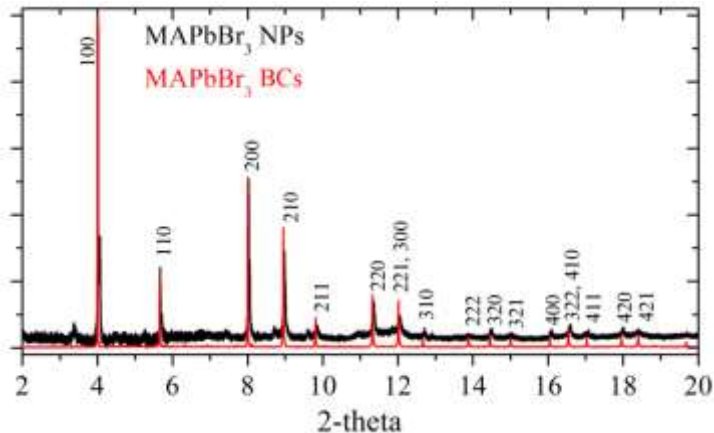


**Figure S1.** XRD patterns of MAPbBr<sub>3</sub> bulk crystals and colloidal NPs

### 3. Size and morphology of MAPbBr<sub>3</sub> nanoparticles

The high resolution transmission electron microscopy (HR-TEM) images reveal the sphere-like morphology of NPs. The crystalline surface can be well-defined with inter-planar distance of 2.98 Å, corresponding to the (002) planes of cubic phase of MAPbBr<sub>3</sub> (Fig. S2a). The histogram of size distribution extracted from the HR-TEM images of the NPs exhibited a mean diameter of 8.2 nm. BCs appear as polygonal disks with thickness of 1.6 μm and mean diameter 15 μm as shown in the SEM image of Fig. S2b. Large-scaled TEM image of the NPs shows that the major part of the sample is nanoparticles Fig. S2c while a minority of 2D nanoplatelets can be found in some area Fig. S2d.

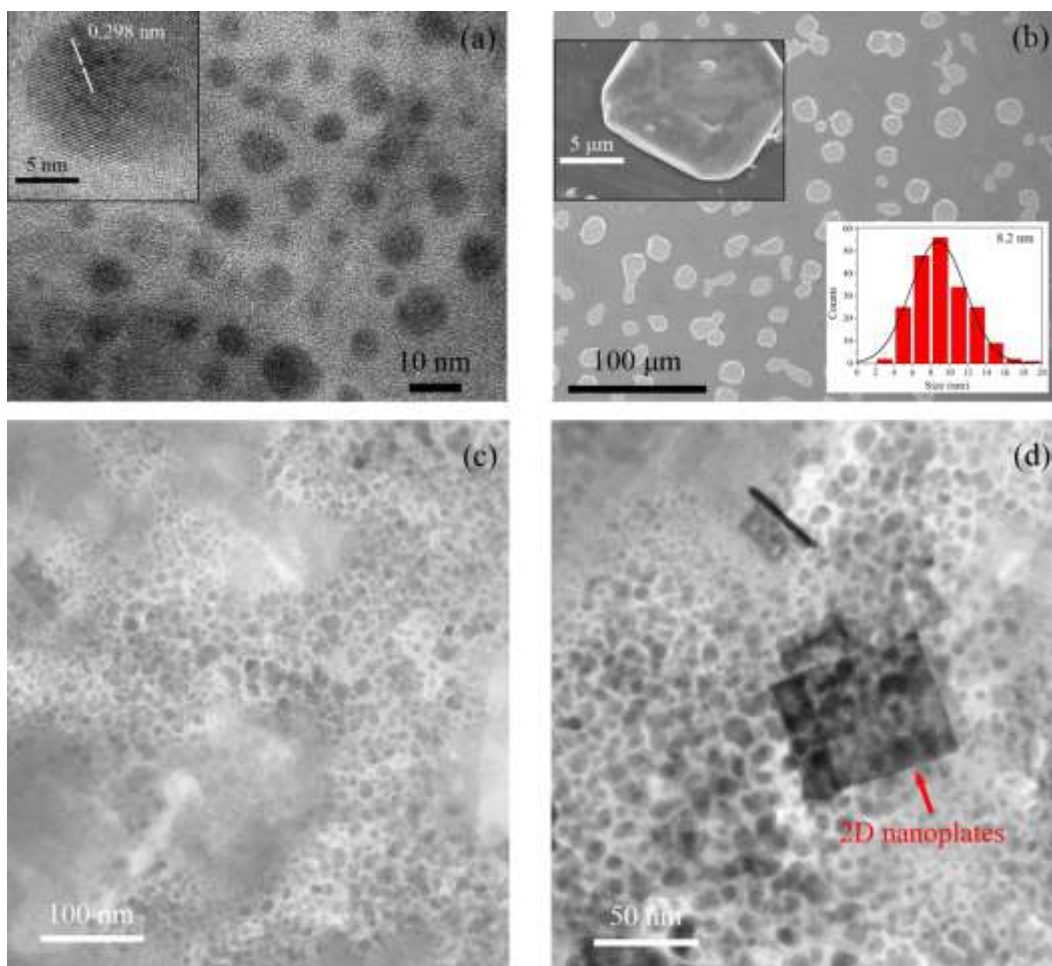


**Figure S2.** (a) The TEM image of as-obtained NPs, the inset shows the atomic layer alignment of one NP. (b) SEM image of the BCs on the glass substrate, the first inset shows the morphology of individual crystal, and the second inset shows the size distribution of the MAPbBr<sub>3</sub> nanoparticles with a mean size of 8.2 nm. (c)&(d) Large-scaled TEM image of the NPs shows that the major part of the sample is nanoparticles while a minority of 2D nanoplatelets can be found in some area (d).

#### 4. Errors of optical band gap calculation:

Due to the possible surface band related tail or light scattering, the extrapolation of the Tauc plots always involves an error. Here we tried two extreme cases (close or away from the absorption tail) to obtain rough errors in the calculated optical band gap values for each sample as shown in Fig. S3. The black extrapolation curves are the ones used in the main text utilizing the major linear part of the Tauc plots. Here we can see that the optical band gap of NPs varies from 2.275 eV to 2.294 eV, while for the BCs from 2.278 eV to 2.292 eV. The errors are subtle (<0.02 eV) and they will not greatly affect the calculation of  $E_b$  in our case.

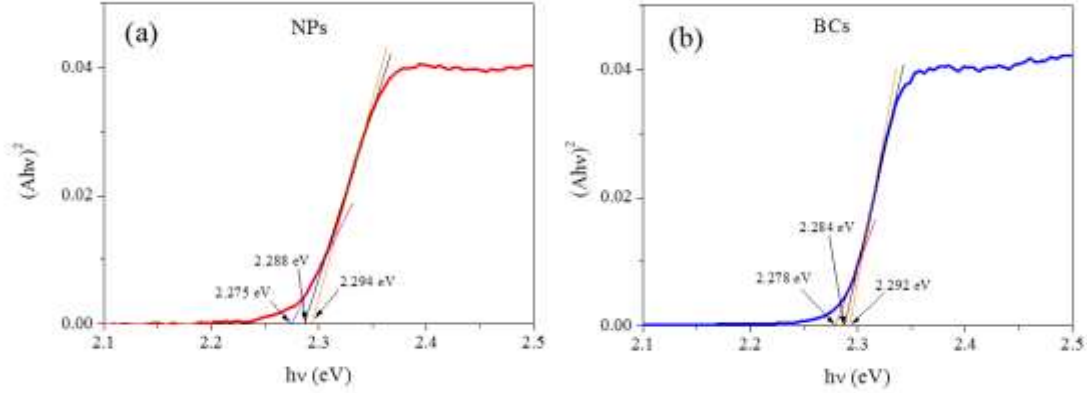


**Figure S3. Tauc plots to determine the optical band gap of (a) the NPs and (b) the BCs.**

### 5. Emission Quantum yield ( $\Phi_f$ ) measurement of MAPbBr<sub>3</sub> NPs:

The relative emission quantum yield of the NPs is determined by comparison to a reference dye (Rhodamine 6G) with known quantum yield as:

$$\Phi_{f,x} = \Phi_{f,st} \cdot \frac{F_x}{F_{st}} \cdot \frac{f_{st}(\lambda_{ex})}{f_x(\lambda_{ex})} \cdot \frac{n_x^2}{n_{st}^2} \quad (1)$$

$$f_{st}(\lambda_{ex}) = 1 - 10^{-A(\lambda_{ex})} \quad (2)$$

where  $\Phi_{f,x}$  is the quantum yield for the quantum dots,  $\Phi_{f,st} = 0.94$  is the quantum yield for the standard dye (Rhodamine 6G),  $F_{st}$  and  $F_x$  are the area under the emission spectrum of the standard dye and the NPs (see Fig. S4a), respectively, and  $n_x = 1.50$  and  $n_{st} = 1.36$  are the refractive index for the QD solvent toluene and the Rhodamine 6G solvent ethanol.  $F_{st}$  is the term correlated to the absorbance of the sample under a given excitation wavelength. During the experiment we controlled the concentration of two samples so that their absorbances are the same as shown in Fig. S4b. Therefore this term can be omitted. Finally,  $\Phi_{f,x}$  was determined as 17%.

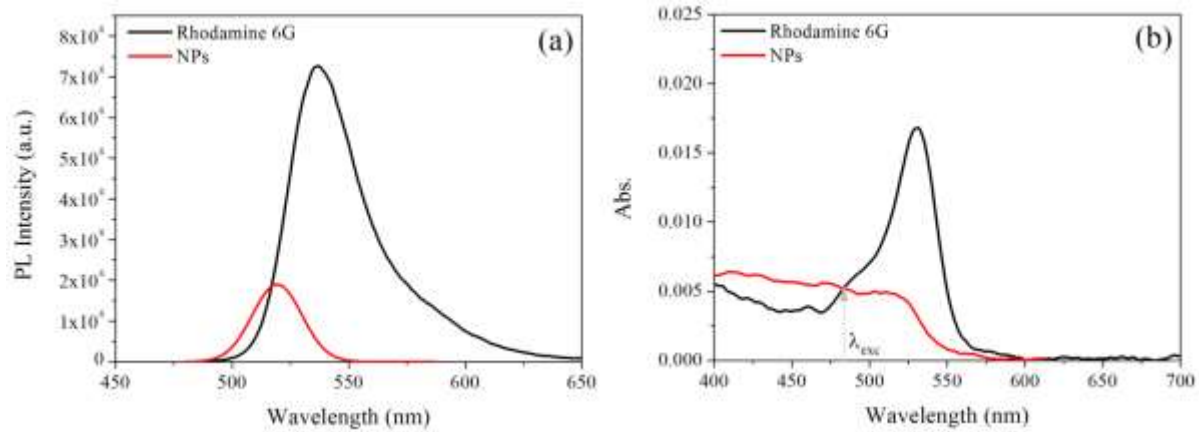


**Figure S4. (a) Emission spectra, and (b) absorption spectra of Rhodamine 6G and MAPbBr<sub>3</sub> NPs.**

## 6. Photoionization cross-sections

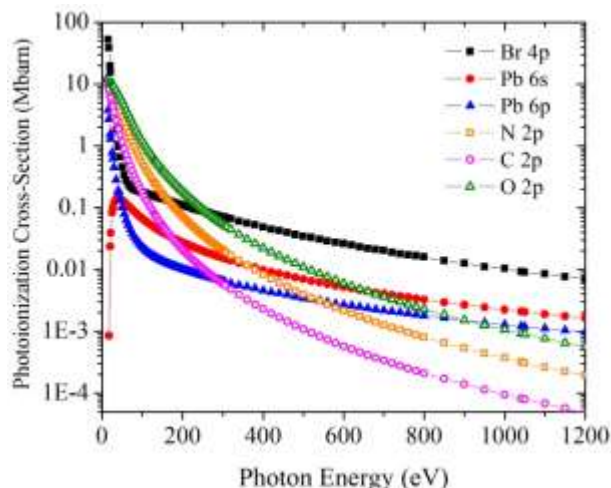


**Figure S5.** The photoionization cross-sections of the possible orbitals contributing to the VB spectra versus photon energy,<sup>2,3</sup> the data shown here are calculated in the dipole length approximation.

## 7. VB surface component:

The VB of the NPs was measured by XPS at PEEM end-station of Beamline I311 of MAX IV laboratory (Sweden) with two different X-ray energies, namely 200 eV and 70 eV, shown in Fig. S6. The sample preparation was the same as for the XPS measurements. The intensities of both spectra were normalized. The escape depth corresponding to the valence electron emission are 8 Å and 5 Å for 200 eV and 70 eV photon energy, respectively, based on the calculation results of PbS powder.<sup>1</sup> Both VB spectra display extra components at lower binding energy, seen from obviously different slopes. At photon energy 70 eV, this extra component is greatly increased compared to the spectra at 200 eV, which means that this component is related to the surface of the sample. Therefore the VBM shown in Fig. 2a is indeed characteristics of the NPs themselves.

Moreover, an obvious tail within 3 - 2 eV is observed for the spectrum of the NPs, which indicates a band ~0.75 eV above the VBM of the NPs. This energy level works as a trap state, and corresponds to the long tail in the absorption spectrum from 550 to 700 nm in Fig. 1. This post-edge absorption tail is commonly attributed to the surface/defect states in semiconductor nanostructures.

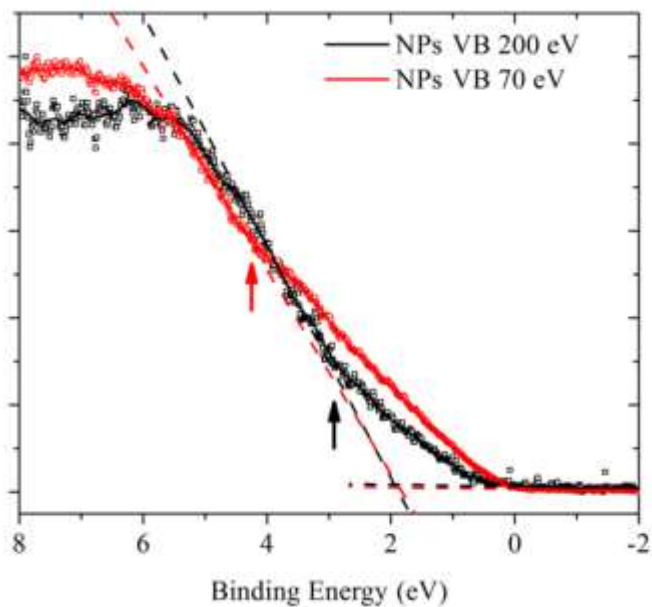
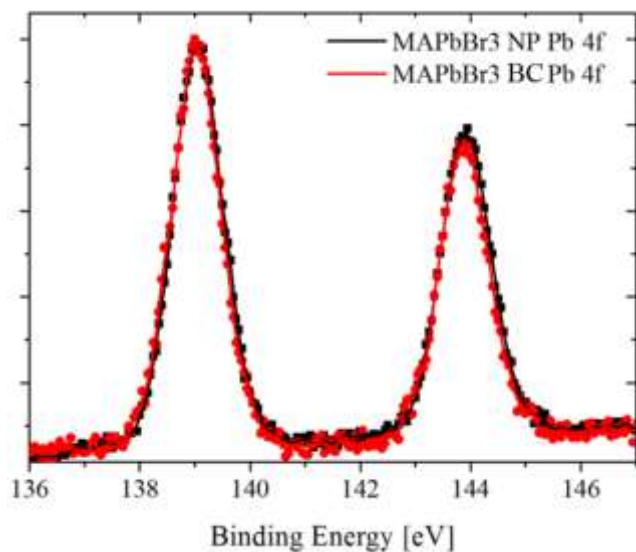


Figure S6. VB of NPs measured by XPS with two different X-ray energies: 200 eV (black) and 70 eV (red).

### 8. XPS core level of NPs:

For this measurement, both the BCs and the NPs samples were used. The fact that the core emission of Pb 4f and 4d of the NPs and the BCs overlap very well (difference  $\leq 0.05$  eV) indicates that no band-bending effect appears due to either metal-semiconductor junction, or the presence of capping agent.



**Figure S7. XPS patterns showing Pb 4f and 4d core levels of the MAPbBr<sub>3</sub> NPs and the BCs with photon energy of 1000 eV.**

### 9. Measure of the E<sub>b</sub> of the BCs sample using temperature dependent photoluminescence

We also evaluated the exciton binding energy of our BCs samples using temperature dependent photoluminescence. PL spectra of BCs were measured at temperatures ranging from 240~350K in a cryostat and the integrated PL intensities  $I(T)$  were calculated. Here the PL intensity decreased with increased temperatures due to the thermal dissociation of excitons at higher temperatures, the temperature dependent PL intensity can then be expressed as follows:<sup>4</sup>

$$I(T) = \frac{I_0}{1 + Ae^{(-E_b/k_B T)}} \quad (5)$$

Where  $I_0$  is the PL intensity at low temperature, and  $k_B$  is the Boltzmann constant. From the linear fitting of  $\ln(I_0/I(T)-1)$  vs.  $1/k_B T$  plot in Fig. S8, we can obtain the  $E_b$  as the slope to be  $84 \pm 10$  meV. This value is close to the reported number 76 meV quoted in the main text considering the experimental error.

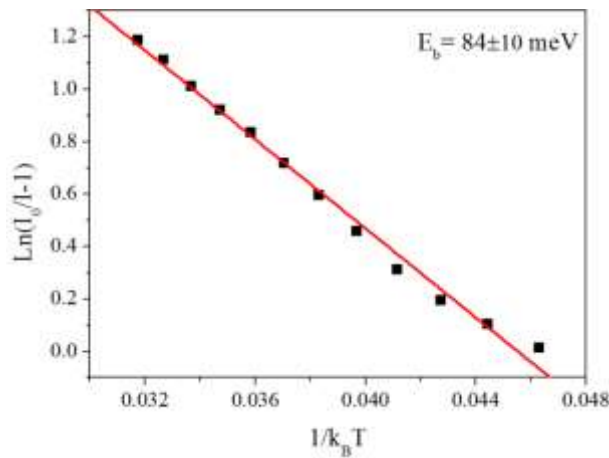


**Figure S8.  $\ln(I_0/I(T)-1)$  vs.  $1/k_B T$  plot of temperature dependent photoluminescence of BCs at temperatures from 240-350 K.**

### 10. Work function measurement:

The work function (WF) of the MAPbBr<sub>3</sub> BCs and NPs were measured at the PEEM end-station of Beamline I311 of MAX IV laboratory. The incident photon energy was 200 eV. The other experimental details are the same as mentioned above for the VB surface component measurements. The experimental results are shown in Fig. S9, the WF of the MAPbBr<sub>3</sub> BCs and NPs are 3.72 and 3.60 eV, respectively.

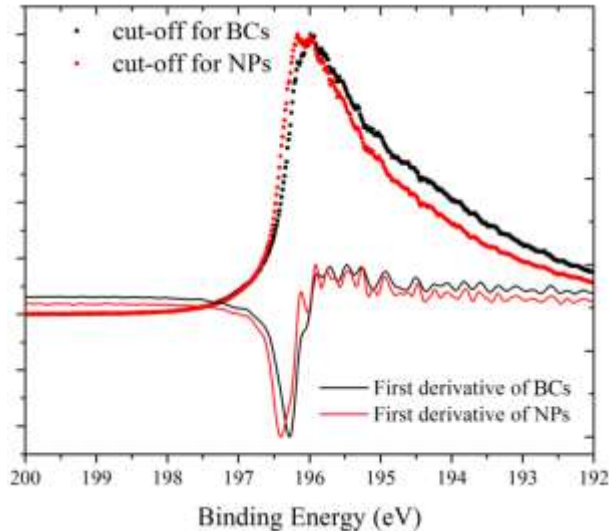


**Figure S9.** Photoemission cut-off for the MAPbBr<sub>3</sub> BCs and NPs, together with the first derivative of each curve. The incident photon energy is 200 eV. The work function (WF) of each sample was fixed by the peak position of the first derivative. The WF of the MAPbBr<sub>3</sub> BCs and NPs are 3.72 and 3.60 eV, respectively.

## 11. Stability and reproducibility of PL kinetics.

In order to verify there is no photochemical reaction which affected the PL dynamics in our case the following test has been conducted for the BCs sample. The PL kinetic was first measured at a flux of 50 nJ/cm<sup>2</sup>, and then the sample was continuous excited at the same excitation intensity for 1h. A PL kinetics at low flux of 5 nJ/cm<sup>2</sup> was required afterwards. After continuous excitation for another 1 h, such cycle was repeated once more. As shown in Fig. S10a, the PL decays almost followed the same trends at both high and low excitation flux. This can prove that no long-term photochemical reaction occurs for our samples and the photodynamics we showed is reproducible and transient. The same photostability can also be observed in NPs sample where the PL kinetics keeps the same for 2h laser excitation at flux of 50 nJ/cm<sup>2</sup>.

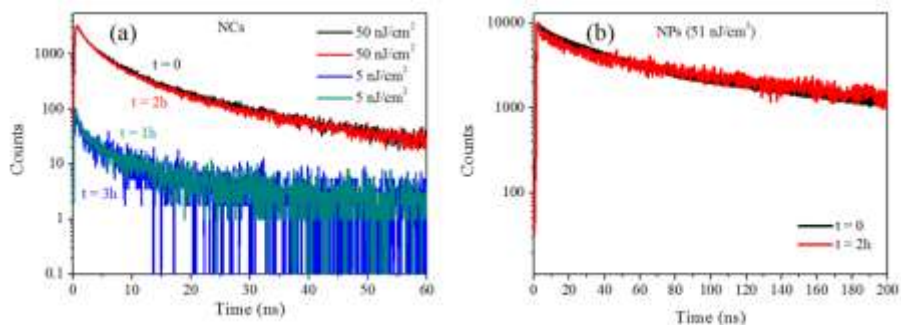


**Figure S10. (a) TRPL kinetics of the BCs at excitation flux of 50 nJ/cm<sup>2</sup> and 5 nJ/cm<sup>2</sup> measured at different times within a continuous laser excitation (50 nJ/cm<sup>2</sup>) in between, and (b) TRPL kinetics of the NPs measured at different times.**

## 12. Calculation of the absorption coefficient and the excitation density of MAPbBr<sub>3</sub>

The absorption coefficient of MAPbBr<sub>3</sub> was evaluated from the absorption spectrum of bulk crystal film with 400 nm mean diameter and 40 nm thicknesses for each crystal. The optical density (O.D.) at 410 nm (the excitation wavelength for time-resolved photoluminescence (TRPL) measurement) is 0.015 as shown in Fig S11.

$$A = \log(I_0/I_1) \quad (1)$$

The morphology of our crystals is disk-like as shown in Fig. S2b, which can be considered as discontinued film. As shown in Fig. S2b, we have such film consisting of discrete crystals with about 12.5% coverage. The OD of a continuous film with the same thickness would be then given as:

$$A_{conti} = \log\left(\frac{I_0}{I_{1conti}}\right) \quad (2)$$

Here  $I_{1conti}$  is the intensity of light after passing through a continuous film, and it can be calculated from the intensity of light transmitted by a discontinued film with 12.5% coverage in our case ( $I_1$ ):

$$I_{1conti} = I_0 - \frac{(I_0 - I_1)}{12.5\%} \quad (3)$$

Then we can get  $A_{conti}$  as:

$$A_{conti} = \log\left(\frac{I_0}{I_0 - (I_0 - I_1)/0.125}\right) = \log\left(\frac{1}{\frac{8}{10^4} - 7}\right) \quad (4)$$

Taking  $A=0.015$ ,  $A_{conti}$  can be calculated as 0.14. The absorption coefficient  $\varepsilon = A/l$ , where  $l$  is the path length of the light which is equal to the thickness of the film 40 nm. We obtain  $\varepsilon = 3.5 \times 10^4 \text{ cm}^{-1}$ .

The excitation density  $n$  can be calculated as the photon flux  $f$  in photons/cm<sup>2</sup> multiplied by the absorption coefficient  $\varepsilon$ :  $n = f\varepsilon$ . The table SI summarizes the corresponding excitation density at different laser photon flux in TRPL measurements:

**Table SI. Excitation density with different laser photon flux**

Power (nJ/cm <sup>2</sup> /pulse)	density	Photon (ph/cm <sup>2</sup> /pulse)	flux	Excitation density (cm <sup>-3</sup> )
0.51		$1 \times 10^9$		$3.5 \times 10^{13}$

5.1	$1 \times 10^{10}$	$3.5 \times 10^{14}$
17	$3.3 \times 10^{10}$	$1.2 \times 10^{15}$
51	$1 \times 10^{11}$	$3.5 \times 10^{15}$

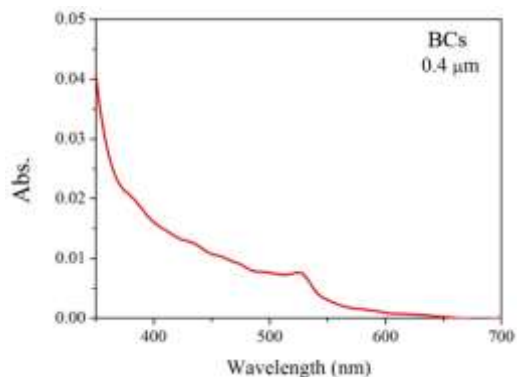


**Figure S11. Absorption spectrum of a MAPbBr<sub>3</sub> bulk crystal film with 400 nm mean diameter and 40 nm thicknesses of each crystal.**

**Reference:**

1. Tanuma, S.; Powell, C. J.; Penn, D. R. *Surf. Interface Anal.* **2011**, *43*, 689-713.
2. Yeh, J. J. Atomic Calculation of Photoionization Cross-Sections and Asymmetry Parameters, Gordon and Breach Science Publishers, Langhorne, PE (USA), **1993**.
3. Yeh, J. J.; Lindau, I. Atomic subshell photoionization cross sections and asymmetry parameters:  $1 \leq Z \leq 103$ , Atomic Data and Nuclear Data Tables, **1985**, *32*, 1-155.
4. Chen, Z.; Yu, C.; Shum, K.; Wang, J. J.; Pfenninger, W.; Vockic, N.; Midgley, J.; Kenney, J. T. Photoluminescence Study of Polycrystalline CsSnI<sub>3</sub> Thin Films: Determination of Exciton Binding Energy. *J. Lumin.* **2012**, *132*, 345-349